New insights into exogenous surfactant delivery to preterm infant lungs: characterization and efficiency of atomization using an *ex vivo* respiratory model

KAOUANE Ghalia[1], BERRET Jean-François[2], CREMILLIEUX Yannick[3], PINAUD Noël[3], MUNSCH Fanny[4], ZHANG Bei[5], FAYON Michael[6], DUMAS DE LA ROQUE Eric[6], GÉRARD Rémy[6], PERINEL Sophie[7], LECLERC Lara[1], POURCHEZ Jérémie[1].

[1]Mines Saint-Etienne, Univ Lyon, Univ Jean Monnet, INSERM, U 1059 Sainbiose, Centre CIS, F - 42023 Saint-Etienne, France.
[2] Laboratoire Matière et Systèmes Complexes, CNRS, UMR 7057, Université Paris Cité, Paris, France.
[3] Institut des Sciences Moléculaires, CNRS, UMR 5255, Université de bordeaux, France.
[4] Institute of Bioimaging, University of Bordeaux, Bordeaux, France.
[5] Canon Medical Systems Europe, Zoetermeer, The Netherlands.
[6] CHU Bordeaux, Département de Pédiatrie, CIC-P INSERM 1401 & Université de Bordeaux, Centre de Recherche Cardio-thoracique de Bordeaux, INSERM U1045, F-33000 Bordeaux, France
[7] Université Jean Monnet Saint-Étienne, INSERM SAINBIOSE U1059, F-42023 Saint-Étienne, France

***CORRESPONDING AUTHOR**
Jérémie POURCHEZ
École Nationale Supérieure des Mines de Saint-Etienne
158 cours Fauriel, CS 62362
42023 Saint-Etienne Cedex 2 - FRANCE.
Email address: pourchez@emse.fr - Telephone number: +33477420180

ABSTRACT

Introduction: The administration of pulmonary surfactant is crucial for the treatment of respiratory distress syndrome (RDS) in preterm infants. The aim of this study is to evaluate the potential of Curosurf® atomization *via* the Endosurf device, a recently developed spray technology, as a promising approach for surfactant delivery in infants with RDS.

Materials and methods: A comprehensive analysis was performed to evaluate the physicochemical properties of atomized Curosurf®, including its surface tension and rheology. The size distribution of atomized Curosurf® vesicles was also investigated. An *ex vivo* respiratory model based on rabbit lungs breathing through an instrumented hypobaric chamber representing the thorax of a preterm infant was developed to provide proof of concept for regional aerosol deposition of atomized Curosurf®.

Results: The atomization of Curosurf® with the innovative Endosurf device did not significantly alter surface tension, but reduced vesicle size and promoted homogeneous distribution of Curosurf® in the lungs. Rheological measurements showed the viscoelastic complexity of atomized Curosurf®.

Conclusion: This preliminary study confirmed the promising potential of Curosurf® atomization *via* the Endosurf device for the distribution of surfactant in the lungs of infants with RDS. These advances could help to improve the treatment of RDS in preterm infants and offer new perspectives for healthcare professionals and affected families.

Keywords: respiratory distress syndrome (ARDS), exogenous surfactant, Curosurf®, surfactant atomization, Endosurf medical device, surface tension, vesicle size, rheology, aerosol deposition, *ex vivo* respiratory model.

1. INTRODUCTION

Premature births represent a major challenge for neonatology. They affect infants born between 22 and 37 weeks of gestation according to the World Health Organization's definition **[1]**. In the mid-twentieth century, the United States struggled with a high infant mortality rate due to preterm birth, which amounted to over 10,000 deaths per year. This led to the discovery of hyaline membrane disease, now known as acute respiratory distress syndrome (ARDS), by Avery and Mead in 1959 **[2, 3]**. ARDS manifests as respiratory distress causing arterial hypoxia **[4]**. Surfactant, which is crucial for efficient breathing, reduces the surface tension of the alveoli. Its production usually begins around the 24th week of gestation and reaches a functional level in the 34th to 36th week. However, premature infants often suffer from surfactant deficiency, which increases their risk of ARDS after birth **[5]**. The incidence of ARDS increases with prematurity. It affects around 1% of all births, but increases to up to 90% in children born before 28 weeks' gestation **[6]**.

The alveoli are crucial for gas exchange in the lungs. They consist of around 480 million tiny vesicles in each lung, which form a huge surface area of 50 to 100 m² **[7][8]**. The alveoli are populated by two cell types, type 1 pneumocytes (AT1) and type 2 pneumocytes (AT2) and are composed of lipids and surfactant-specific proteins **[9] [10]**. Although they account for only 10% of alveolar cells, AT1 cells cover 90% of the alveolar surface and facilitate gas exchange by diffusion **[11]**. AT2 cells, which make up about 15% of alveolar cells, produce pulmonary surfactant, which is mainly composed of phospholipids and proteins and forms a thin layer (100-500 nm thick) on the alveolar surface. This surfactant reduces surface tension, which is crucial for maintaining alveolar stability during respiration.

In vivo, the presence of pulmonary surfactant ensures a balanced pressure distribution and prevents atrophy of smaller alveoli and hypertrophy of larger alveoli (Supplementary Data **S1**). This balance promotes effective gas exchange by mitigating the effects of capillarity and maintaining alveolar stability, which is critical for respiratory function.

The lipid component, which makes up about 90% of the surfactant composition, consists mainly of phospholipids, with phosphatidylcholine being the most abundant, especially dipalmitoylphosphatidylcholine. Proteins make up about 10% of the surfactant content. The surfactant synthesized by the AT2 pneumocytes first forms compact bilayers, the so-called lamellar bodies, which serve as a reservoir before it is released into the hypophase. The reduction of surface tension is favored by the interaction of lipids and proteins, which is crucial for lung health of the lungs and the efficiency of gas exchange. Pulmonary surfactant can be inactivated by several mechanisms that contribute to or result from various diseases **[12]**.

Endogenous pulmonary surfactant is obtained by bronchoalveolar lavage, which is performed in living mammals by bronchoscopy, an invasive procedure, or in sacrificed animals. In addition to ethical considerations, the quantities of endogenous surfactant obtained are small, and damaged lungs can lead to contamination with cellular material **[12]**. This complexity necessitates the use of exogenous pulmonary surfactant as an alternative, which is obtained from various sources. Commonly used animal surfactants include beractant "Survanta®" and calfactant "Infasurf®" from bovine lungs and poractant alfa "Curosurf®" from porcine lungs. These substitutes differ not only in lipid and protein concentration, but also in vesicle structure **[13,14,15,16]** and rheology **[17,18,19,20,21,22,23]**. Curosurf® has a higher concentration of phospholipids and requires a lower administration volume and is therefore used in hospitals for the treatment of ARDS **[24]**.

Techniques for administering exogenous surfactant have evolved to better meet the needs of preterm infants with ARDS. Originally, surfactant was administered to mechanically ventilated preterm infants, but this often resulted in prolonged ventilation and did not effectively reduce bronchopulmonary dysplasia **[25]**. Currently, the most commonly used method is instillation of surfactant and rapid extubation **[26]**. Despite its popularity, instillation of surfactant can lead to problems during extubation, resulting in prolonged mechanical ventilation **[27]**. An alternative approach, known as less invasive surfactant administration (LISA), involves administering surfactant *via* a feeding tube or small catheter while the infant is breathing spontaneously. This method minimizes the need for invasive ventilation. Studie have shown that LISA can shorten the duration of mechanical ventilation and reduce the incidence of chronic lung disease in preterm infants **[28]**. Ongoing research aims to develop even less invasive methods such as nebulization or surfactant nebulization. Nebulization offers potential benefits, including more uniform distribution and less reliance on mechanical ventilation. However, further clinical studies are needed to fully evaluate these techniques **[25]**. Preliminary results from a pilot study suggest that delivery of aerosolized surfactant via nasal continuous positive airway pressure (nCPAP) is a viable and safe option **[29]**.
The aim of this work is to characterize and evaluate the performance of atomization of exogenous surfactant using an innovative spray technology to overcome the challenges in the treatment of preterm infants with ARDS. A team of neonatologists, pediatric pulmonologists and French start-up companies have developed the patented concept of the Endosurf medical device **[30]**. This innovative device aims to (i) avoid the painful laryngoscopy required for the LISA technique, (ii) deliver surfactant by atomization to achieve a better distribution in the lungs with a lower surfactant volume, and (iii) provide a more user-friendly learning curve compared to the LISA technique. In this study, we will investigate whether atomization with the Endosurf technology changes the physicochemical properties of the exogenous surfactant such as surface tension, rheology, vesicle size and structural properties of the Curosurf® vesicles. In addition, proof of concept for regional aerosol deposition of surfactant in the lung is provided using an *ex vivo* respiratory model based on a heart-connected rabbit thorax breathing through an instrumented hypobaric chamber mimicking a preterm infant.

1. MATERIALS AND METHODS

1.1. Physicochemical features of exogenous surfactant pre- and post-atomization

In our study, we used the patented concept of the medical device Endosurf **[30]** to atomize the surfactant Curosurf®, Chiesi Farmaceutici, Parma, Italy. For these experiments, this device was coupled with a high-pressure aspirator of the 3340 series (INSTRON®, Élancourt, France), which allows precise movement at a constant speed of 500 mm/min over a distance of 120 mm and ensures controlled atomization. Before atomization, the Curosurf® was heated to 37°C to reach physiological temperature. Three different devices were used for the tests, each operating at a specific atomization pressure. Each Curosurf® vial, lot number 1154081, initially contained 2.5 mL of the product, with 0.5 mL reserved as a blank control (**Table 1**). After atomization, the samples, whether nebulized or not, were stored at 4°C for subsequent analysis of their physicochemical properties.

Table 1: *Summary Table of Atomized / Non-atomized Curosurf® Volumes and pressure.*

Endosurf device number	Pressure applied (bar)	Batch number of Curosurf®	Surfactant volume (mL)	Volume of surfactant loaded in the syringe(mL)	Volume of recovered surfactant after atomization (mL)	Non-atomized Curosurf® (mL)
(1)	59.5	1154081	3	2.5	2	0.5
(2)	30.9		3	2.5	2	0.5
(3)	75.8		3	2.5	2	0.5

There are different approaches to evaluate the change in physicochemical properties of Curosurf® intended for administration to preterm infants: measurement of surface tension, rheological analysis, structure and size of surfactant vesicles.

1.1.1 Surface tension measurement

One of the basic physico-chemical properties of surfactants is their ability to equalize the surface tension between alveoli and air. Surface tension was characterized for both forms of exogenous surfactant solution (Curosurf®): atomized and non-atomized, using the hanging drop method with the Digidrop DX device from GBX Scientific LTD (Romans-sur-Isère, France). This device allows the measurement of contact angle, wettability, surface energy and surface tension by a hanging drop. The method is based on the equilibrium shape of drops, where small drops tend to be spherical due to surface tension effects that minimize the surface area of the drop. Gravity effects, which are influenced by the volume of the drop, can lead to distortions. If surface tension and gravity are in balance, the surface tension of a liquid can be determined from the resulting drop shape. This method is often used because it requires only a small amount of liquid and quickly provides an accurate measurement of surface tension. The general procedure is to use a needle to form a droplet in equilibrium just before it separates. Some of its dimensions are then measured using digital image processing. Surface tension measurements were performed at room temperature (+20°C), in three replicates for each atomized Curosurf® sample (Endosurf device (1), (2) and (3)) and in six replicates for pooled, non-atomized Curosurf® (**Figure 1**). The droplet profile is analyzed, including volume, angle and base diameter. Based on the density of Curosurf® at +20°C, which is 1.0018, and the collected data, the surface tension is calculated.
The Curosurf® drops are collected in a vial below the needle and stored at +4°C for further rheological analysis.

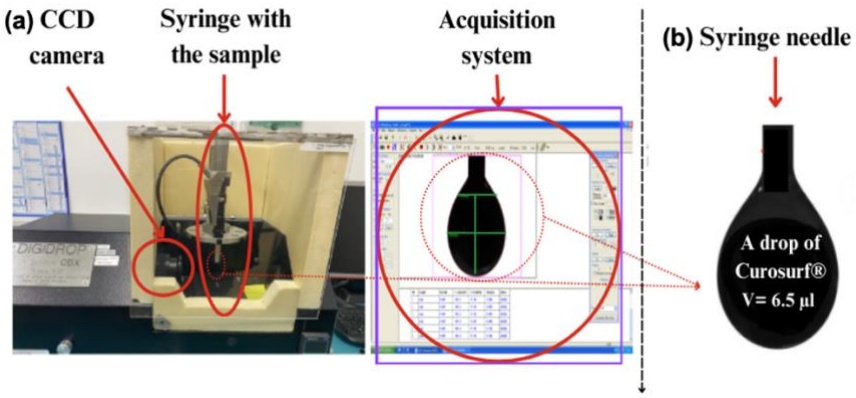

Figure 1: *Measurement of surface tension using the hanging drop method.*

(a) Tensiometer (Digidrop DX device from GBX Scientific LTD): This device consists of a light source, a CDD camera, a platform and a dosing unit with a syringe. (b) Image of a Curosurf® pendant drop in air attached to the syringe needle.

2.1.2 Cone-and-Plate rheology

The rheological experiments were carried out using a RheoCompass MCR 302 rheometer (Anton Paar SAS, Courtaboeuf, France) equipped with a cone and a plate with a diameter of 50mm and a cone angle of 1°, as well as a solvent trap to minimize water evaporation. Measurements of the complex modulus $G^*(\omega) = G'(\omega) + iG"(\omega)$, where $G'(\omega)$ and $G''(\omega)$ are the elastic and loss moduli, were recorded as a function of the strain γ_0 and the angular frequency ω through strain and frequency sweeps, respectively. In strain sweeps, the angular frequency was held constant at 1 rad s^{-1} while varying the applied strain γ_0 from 0.1 to 100%. For all Curosurf® samples tested, we found a linear regime below the deformation γ_0 = 10%. Moduli were hence measured at the slightly lower strain of 5%. In frequency sweeps, the angular frequency was varied between 0.1 and 100 rad s^{-1}. Both atomized and non-atomized Curosurf® samples were evaluated following the same experimental procedures. Each sample's cone-and-plate measurements were conducted in duplicate at a temperature of +37°C (**Figure 2**).

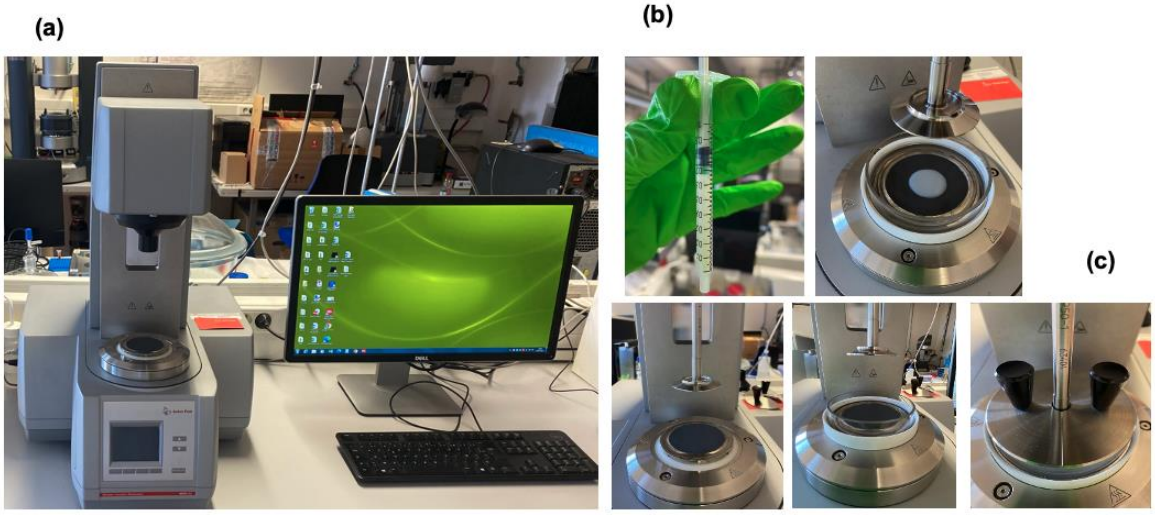

Figure 2: *Measuring the viscosity of atomized and not atomized Curosurf®.*
(a)The viscosity was determined with the Physica RheoCompass MCR 302 from Anton Paar using a cone and plate geometry with a diameter of 49.957mm and a cone angle of 0.997. (b)A sample volume of 0.65mL was used. The rheological measurements were performed on both atomized and non-atomized Curosurf® samples. (c)Accessories were used to prevent evaporation of the samples, which were stored at a temperature of +37°C.

2.1.3 Optical microscopy

For direct visualization of the Curosurf® vesicles, an inverted microscope IX73 (Olympus SAS, Rungis, France) with an x60 objective (numerical aperture 0.70) was used, allowing brightfield and phase-contrast imaging [**31, 32**]. The data acquisition system consisted of an EXi Blue CCD

camera (QImaging, Surrey, Canada) with Metamorph (Universal Imaging Inc., Bedford Hills, USA). For this study, four samples of the exogenous surfactant were analyzed, including one sample before atomization and three samples after atomization at different magnifications (x20, x40 and x60). In the method, 2 µl of the sample was placed between two 16 mm diameter round coverslips held together with a homemade screw clamp system (**Figure 3.d**). A stream of air, which was directed into the measuring cell through an air inlet cover, was used to heat the sample to +37°C. The vesicle images were digitized and processed using ImageJ Fiji software and plugins **[33]** for structural analysis, including determination of vesicle size. Only the phase contrast images with 60x magnification are shown, which allow better visualization and individualization of the vesicles.

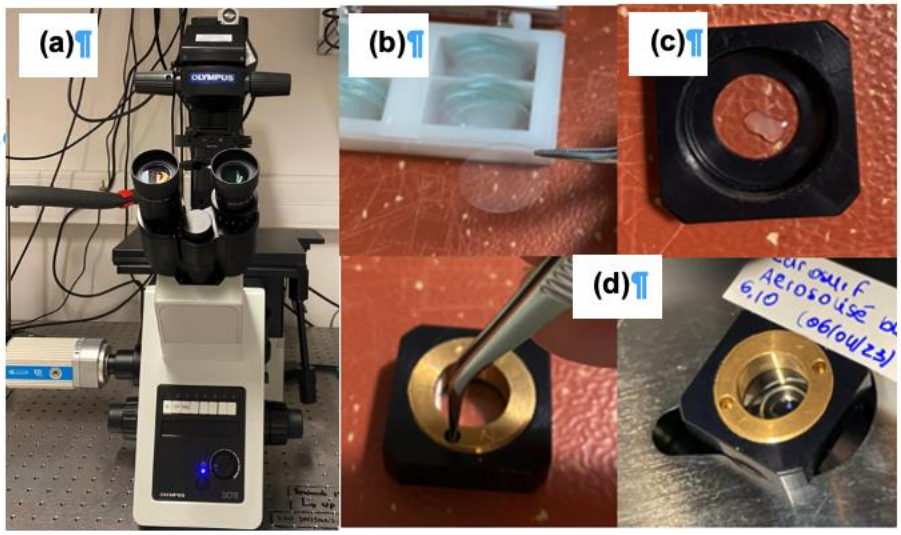

Figure 3: *Microscopic Observation and Analysis of Samples Using Phase-Contrast (PC) and Bright-Field (BF) Techniques.*
(a) Olympus IX 73 inverted microscope utilized for imaging; (b) 16 mm diameter round coverslip employed as the sample substrate; (c) 2 µL of Curosurf® carefully deposited onto the coverslip for analysis; (d) screw clamp system used to securely mount the sample during observation.

1.2. Aerodynamic parameters of atomized surfactant using the SPRAYTEC device

We measured the particle size distribution (PSD) of aerosol droplets using the SPRAYTEC laser diffraction technique (Malvern Panalytical, Palaiseau, France). An open laser beam (range 0.5-900µm) generated with a 300F lens –was used to analyze the droplets after 15 seconds of atomization. The laser diffraction instrument determined the size distribution by measuring the angular variation of the scattered light intensity, creating a diffraction pattern. The PSD was characterized by the mean mass diameter (D (0.5)), which indicates the size at which 50% of the sample is smaller and 50% is larger. The values given are averages of at least three determinations.
Nine Endosurf devices were used to determine the PSD of the generated spray (**Table 2**), using the same method as in the previous section (Physico-chemical properties of the exogenous surfactant before and after atomization).
Table 2: *Summary Table of Atomized Curosurf® Volumes and Pressure.*

Endosurf device number	Pressure applied (bar)	Batch number of Curosurf®	Surfactant volume (mL)	Volume of surfactant loaded in the syringe(mL)	Volume of recovered surfactant after atomization (mL)	Non-atomized Curosurf® (mL)
(4)	40	1162353	3	2.5	2	0.5
(5)	35	1162353	3	2.5	2	0.5
(6)	35	1162353	3	2.5	2	0.5
(7)	35	1163893	3	2.5	2	0.5
(8)	35	1170710	3	2.5	2	0.5
(9)	30	1170710	3	2.5	2	0.5
(10)	NA	1170710	3	2.5	2	0.5
(11)	20	1154081	3	2.5	2	0.5
(12)	27.5	1154081	3	2.5	2	0.5

1.3. *Ex vivo* respiratory model and MRI imaging of surfactant distribution in the lungs.

The identification of deposition sites plays a crucial role in the assessment of tissue doses and subsequent biological effects. An innovative methodological approach based on *ex vivo* imaging experiments was chosen. Anatomical models of animals intended for human consumption were used. These experiments were performed on anatomical rabbit models obtained from food industry waste and follow the 3R principles (Replacement, Reduction and Refinement). The dissected rabbit thoraxes were placed in an instrumented hypobaric chamber used to mimic pleural depression **[34]**. Thus, lungs were ventilated similarly to *in vivo* passive ventilation. Besides, a neonatal ventilator (Babylog, Draeger, Lübeck, Germany) was connected to the trachea to maintain a continuous positive airway pressure fixed at 6 cmH_2O. A solution of exogenous surfactant and contrast agent was prepared by mixing 2.7 ml of a clinically used surfactant Curosurf ® and 0.27 ml of a gadolinium-based contrast agent (Dotarem, Guerbet, Villepinte, France). The solution was heated in a water bath at +37°C for 5 to 10 minutes. Subsequently, 2.5 ml of the solution was placed in the Endosurf device at body temperature. The device was inserted into the trachea of the lung and the solution was nebulized within a few seconds. The chamber was then placed in the center of the MRI magnet for the acquisition of MR images.

MRI scans were also performed on an isolated rabbit thorax after 2.7 ml of surfactant solution was mixed with 0.27 ml of gadolinium-based contrast agent, pre-warmed to +37°C and instilled into the rabbit lung using the LISA reference method. MRI scans were performed using a clinical 3T whole-body magnet (Vantage Galan 3T ZGO, Canon Medical Systems Corporation, Japan). MR images were acquired using a 3D MRI sequence with ultra-short reverberation time (UTE) and the following acquisition parameters: Repetition time = 3.7ms, echo time =

96µs, 1 mean, total acquisition time = 3min28sec, field of view = 11.3x11.3cm^2, slice thickness = 1mm, voxel size = 0.78x0.78x1mm^3 **[35]**.

1. RESULTS AND DISCUSSION

1.1. Comparison of physicochemical features of exogenous surfactant pre- and post-atomization with the Endosurf spray device

1.1.1 Surface tension

The results show an average surface tension of 30.0 ± 1.405 mN m^{-1} for the non-atomized surfactant and 31.3 ± 1.46 mN m^{-1} for the atomized surfactant (**Figure 4**). An unpaired Student's t-test revealed no statistically significant difference between the two groups (p = 0.3156), indicating that atomization did not significantly alter the surface properties of the exogenous surfactant. In addition, the coefficient of determination (R^2 = 0.07732) indicates that only a small part of the variance in surface tension is explained by atomization. This weak correlation confirms that atomization has only a minimal effect on the surface tension of the surfactant.

Surface tension was measured using the hanging drop method at +20°C for both atomized and non-atomized surfactants to evaluate the effects of atomization on their physicochemical properties. As shown in **Figure 4**, the average surface tension was 30.0 ± 1.405 mN m^{-1} for the non-atomized surfactant and 31.3 ± 1.46 mN m^{-1} for the atomized surfactant. The results of the t-test confirm the finding that atomization does not significantly influence the surface tension. In addition, the low R^2 value (0.07732) indicates a negligible correlation between atomization and the measured surface tension values.

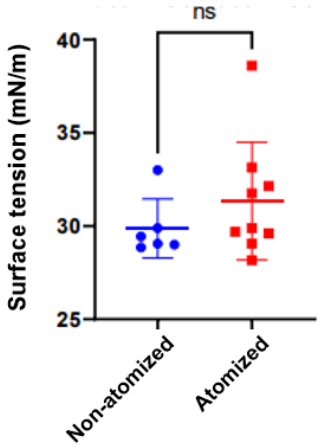

Figure 4: *Comparison of the surface tension (mN/m) between atomized and non-atomized exogenous surfactant. Surface tension of each drop is plotted with the error bars representing the standard deviations.*

Previous measurements using the captive bubble method at +37°C gave a surface tension of 36.4 mN m^{-1} for the non-atomized exogenous surfactant **[36]**, suggesting that differences in method and temperature may influence the results. Although the difference between the two groups did not reach statistical significance (p=0.32), atomization did not result in a significant increase in the surface tension of the exogenous surfactant, which is supported by current and previous data and reinforces confidence in its use in the treatment of respiratory distress syndrome.

3.1.2 Rheological properties

Strain and frequency sweep measurements were first performed on freshly opened Curosurf® batches. Once loaded into the tool geometry, the samples were measured sequentially two or three times to test the reproducibility of the measurements over time. **Figure 5a** shows the frequency dependence of the elastic and loss moduli for two freshly opened samples (batch number 1162353). Under the used conditions, the measurement was made within minutes after opening the flask. In **Figure 5a** it can be seen that the two measurements gave similar results, with data points largely superimposed over the entire frequency range. A second observation is that the elastic and loss moduli are close to each other, with values of the order of 0.05Pa at 1rad s^{-1}. This indicates viscoelastic behavior, with a low elastic contribution. The rheological response shows power-law dependences of the form $G'(\omega) \sim \omega^{\alpha}$ and $G''(\omega) \sim \omega^{\beta}$, with exponents α = 0.38 ± 0.02 and β = 0.56 ± 0.02. In line with the results obtained for fluids undergoing a sol-gel transition, the exponent values indicate that Curosurf® at 80 g L^{-1} is below the sol-gel transition, which is characterized by a rheological state where $G'(\omega) > G''(\omega)$ with both α and β of the order of 0.7 **[37-39]**. Compared with the data from Ciutara et al. who also carried out elastic and loss modulus measurements on Curosurf® **[40]**, $G'(\omega)$ and $G''(\omega)$ values measured here are lower by a factor of 2. It should be added that Ciutara *et al.* [**40]** also found $G'(\omega) > G''(\omega)$ over the 0.5-10rad s^{-1} measurement range, leading the authors to conclude that Curosurf® at 80g.L^{-1} was in a gel state. With regard to the Curosurf® linear rheology, we find slightly different results from those of Ciutara *et al.* **[40]** and Thai *et al.* **[32,41]**. In contrast, we observe a crossing of the curves $G'(\omega)$ and $G''(\omega)$ around the frequency of 3 rad s^{-1}, with $G'(\omega) > G''(\omega)$ before and $G''(\omega) > G'(\omega)$ after.
To determine the long-term stability of Curosurf® physical properties over time, and in particular their viscosity properties, $G'(\omega)$ and $G''(\omega)$ were measured on the same sample shortly after opening the bottle, after one day, and after one month (**Figure 5b**). Between these measurements, the sample was kept at +4°C in the dark. We observed that after one day the results were similar to those for the freshly opened sample. However, after one month, there was a significant change in the frequency behavior of the complex elastic modulus $G^*(\omega)$, with the elastic modulus increasing by a factor of 20 and the loss modulus by a factor of 10 with respect to the initial sample. Additionally, $G'(\omega)$ exceeded $G"(\omega)$, and the frequency behaviors had exponents α = 0.07 and $\beta \sim 0$, clearly indicating a gel-like behavior **[37,42**]. The increase in elastic modulus seen in **Figure 5b** could be due to chemical modification of the lipids or proteins present in the dispersions, leading to the formation of a percolation network of vesicles. These measurements suggest that the aging effects of Curosurf® occurred over a time scale of one month, and that precautions should be taken when measuring exogenous pulmonary surfactants **[32,37,40,41,43-46]**.

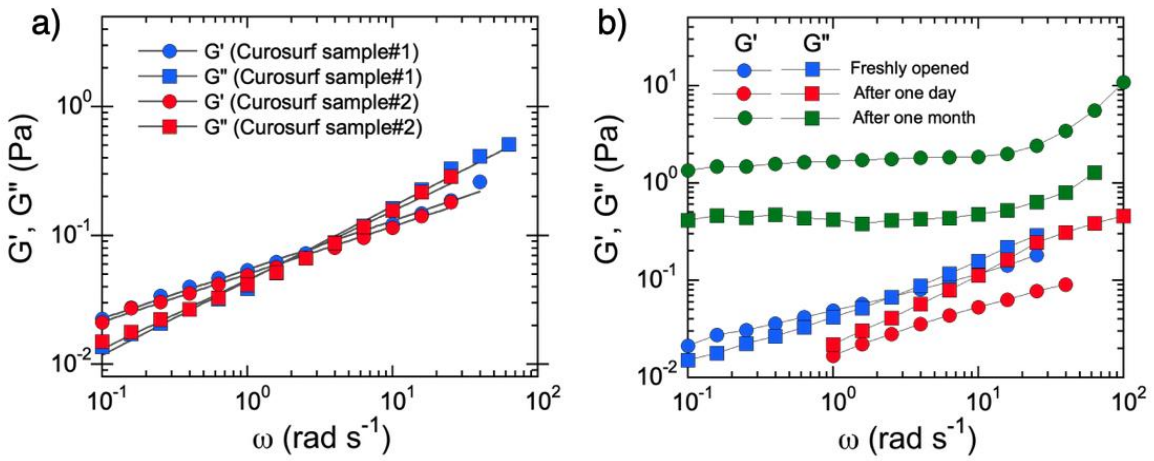

Figure 5: *A) Elastic and loss moduli of freshly opened Curosurf® samples as a function of the angular frequency (T = +37°C).*
The cone-and-plate measurements were performed in the linear regime of deformation (γ_0 = 5%). The straight lines through the data points result from best-fit calculations using power-law functions of the form $G'(\omega) \sim \omega^{\alpha}$ and $G''(\omega) \sim \omega^{\beta}$, with exponents α = 0.38 and β = 0.56. B) $G'(\omega)$ and $G''(\omega)$ obtained from a Curosurf® sample shortly opening, after one day and after one month. After opening, the dispersion was kept at +4°C in the dark. The plateau in modulus $G'(\omega)$ after one month suggests viscoelastic gel behavior.

Figure 6 compares the linear viscoelastic behaviors of samples originating from the same batch (number 1154081) atomized using different versions of the Endosurf prototypes. These prototypes are termed Device (1) (**Figure 6a-b**), Device (2) (**Figure 6c-d**), and Device (3) (**Figure 6e-f**) respectively. The upper panels show the elastic moduli, while the lower panels display the loss modulus. For most data collected, $G'(\omega)$ and $G''(\omega)$ exhibit moduli around 0.05–0.1Pa, similar to those of freshly opened samples. The continuous blue lines for $G'(\omega)$ and red lines for $G''(\omega)$ represent the power laws obtained from freshly opened flasks (**Figure 5a**), with α and β being 0.38 and 0.54, respectively. The data obtained before and after atomization show good agreement, except for those in **Figure 6c** at high frequencies. In some cases, there is even an overlap between non-atomized and atomized samples (**Figure 6b, 6e, 6f**). These data indicate that the rheological properties of the atomized Curosurf® samples are similar to those of the initial samples, confirming the potential use of Endosurf devices for the delivery of exogenous surfactants to humans.

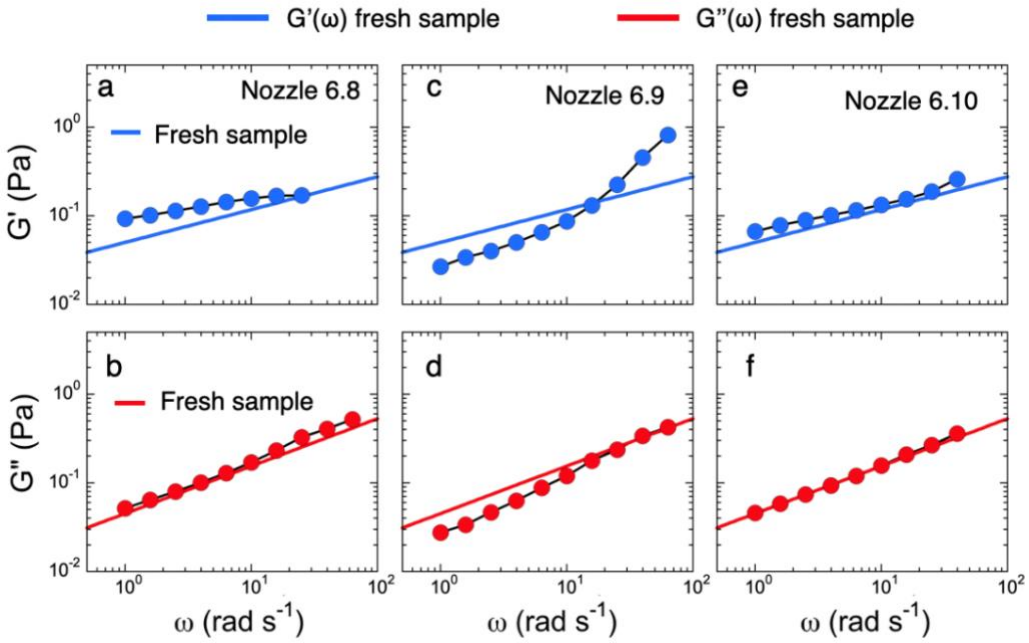

***Figure 6**: Elastic (upper panels) and loss (lower panels) modulus of a Curosurf® sample atomized through 3 different Endosurf prototypes.*
These prototypes are labelled Device (1) (a-b), Device (2) (c-d), and Device (3) (e-f) respectively. The experiments were carried out in the linear regime of deformation (γ_0 = 5%) and at +37°C. The solid lines show the results for the non-atomized sample, for comparison.

3.1.3 Structure and size of surfactant vesicles

a) Phase contrast microscopy

Phase contrast microscopy was used to evaluate the effects of atomization on the morphology of the exogenous surfactant vesicles (**Figure 7**). The main objective was to compare the morphological features and size profiles of the vesicles between the non-atomized exogenous surfactant (Figure 7 - image a) and the atomized counterparts (Figure 7 - images b, c and d).

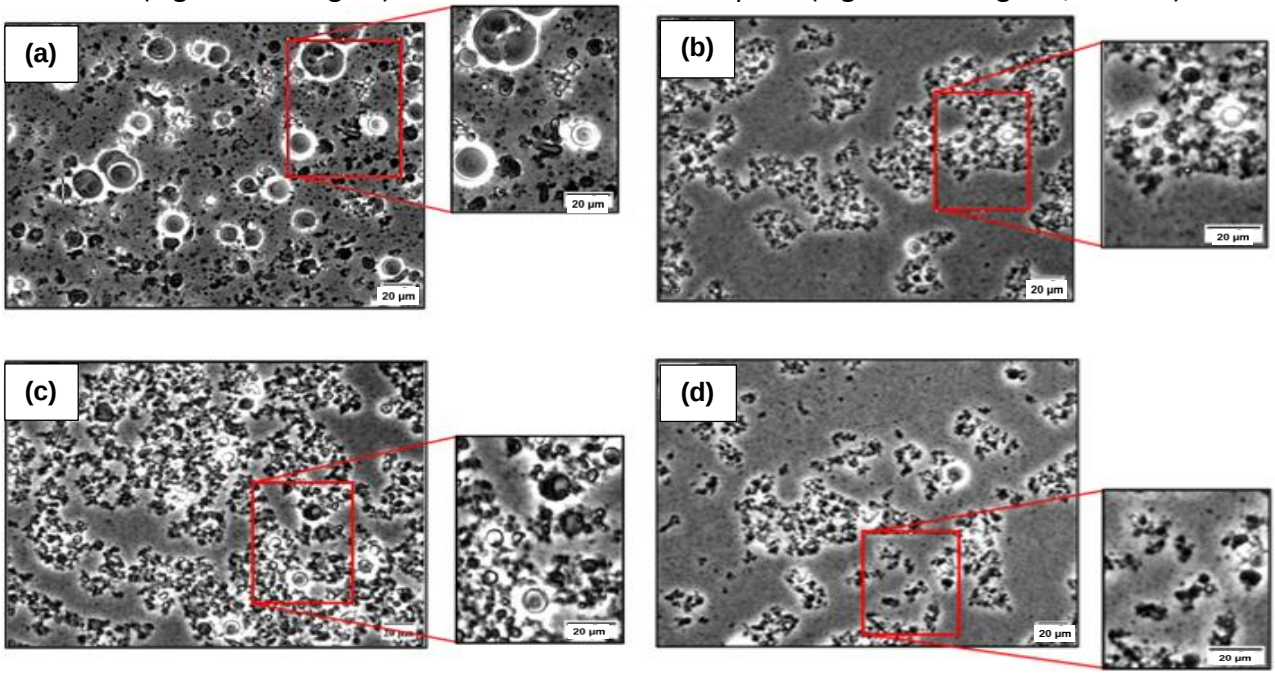

***Figure 7**: Microscopic images of exogenous surfactant*
Fresh, non-atomized exogenous surfactant (image a) and atomized with Endosurf devices (1), (2) and (3) (images b, c and d). The images were taken with the Olympus IX73 microscope with phase contrast and processed with ImageJ Fiji software (magnification ×60, scale bar = 20 µm).

Visual inspection of the microscopic images reveals a difference in the size of the vesicles between the non-atomized exogenous surfactants and their atomized counterparts. To quantitatively delineate this difference, precise measurements of the average vesicle size were performed in representative image areas (**Table 3**). The results show that the average size of the vesicles in the non-atomized exogenous surfactants is about 2.2 µm, which is almost twice as large as that of the atomized vesicles, which is about 1.1 µm.

Images	Number of vesicles	Average diameter (µm)	Max value (µm)	Min value (µm)	Standard deviation
(a) non-atomized)	273	2.2	17.1	0.1	2.4
(b) Device 1	781	1.0	8.6	0.1	0.8
(c) Device 2	327	1.3	12.3	0.2	1.3
(d) Device 3	685	1.0	5.9	0.2	0.9

***Table 3**: Summary of measurement of diameter/number of exogenous surfactant vesicles.*
Other remarkable observations concern the frequency of the vesicles. The number of small bubbles is significantly higher in the atomized samples than in the non-atomized samples. If we compare Image (a) and Image. (b), we can see that although the surface area covered by the vesicles remains more or less the same, the number of vesicles increases. Image (a) shows about 273 vesicles, while Image (b) shows 781 vesicles (about 2.8 times more).

b) Distribution of vesicle sizes of exogenous surfactants before and after atomization

This study presents the results of analyzing the size distribution of exogenous surfactant vesicles, where a total of 250 vesicles were examined for each sample condition (see **Supplementary Data S2**). The aim was to compare the size distribution between non-atomized and atomized samples. The results were analyzed using GraphPad Prism software (Boston, Massachusetts, USA), which facilitates the visualization of size differences between vesicles.

Figure 8 shows significant differences in the size distribution of the vesicles before and after atomization. The mean vesicle diameter for the non-atomized sample is 1.33 µm, accompanied by a wide distribution range extending up to 6 µm, indicating considerable heterogeneity within the non-atomized sample. In comparison, the mean diameters of the atomized samples were significantly smaller, with values between 0.67 µm and 0.84 µm for the three different atomization devices (devices 1, 2 and 3).

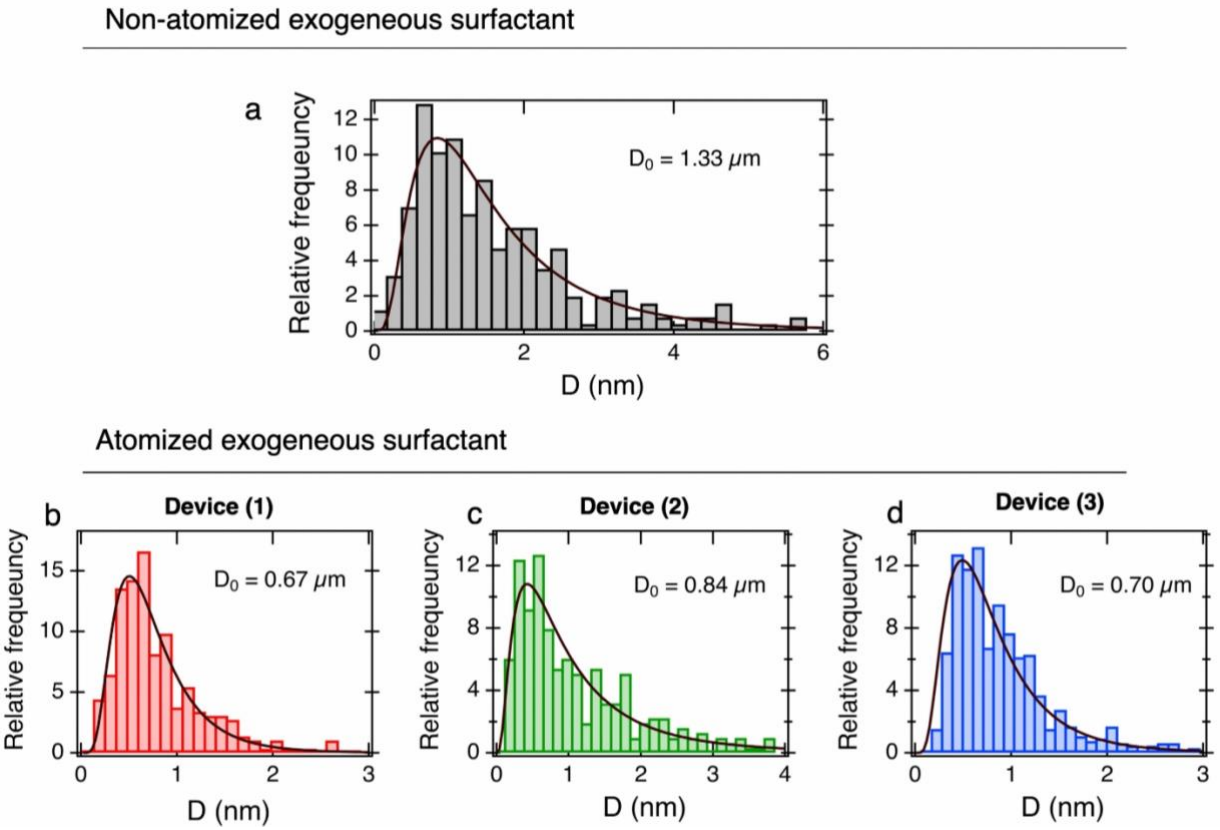

Figure 8*: Distribution of the vesicle size of the exogenous surfactant before and after atomization.*

(a) *Relative frequency distribution of vesicle diameters (D) in the non-atomized sample, with a mean diameter* $D_0 = 1.33\mu m$*.(b–d) Relative frequency distributions of vesicle diameters for three different atomization devices:* ***(b)*** *Device (1),* $D_0 = 0.67\mu m$*;* ***(c)*** *Device (2),* $D_0 = 0.84\mu m$*; and* ***(d)*** *Device (3),* $D_0 = 0.70\mu m$*.*

The atomized samples consistently had smaller vesicle diameters than the non-atomized samples. For example, the average vesicle diameter of the sample atomized with Device 1 was 0.67 µm, highlighting the effectiveness of atomization in reducing vesicle size. In addition, the atomized samples exhibited lower standard deviations, indicating a more uniform size distribution of the measured vesicles. Optical phase contrast microscopy also showed remarkable differences in the morphology and size distribution of the vesicles. The non-atomized vesicles had an average size of 1.33 µm, while the average size of the atomized vesicles was significantly smaller at about 0.75 µm. This drastic reduction in size illustrates the mechanical fragmentation that occurs during atomization, whereby larger vesicles are broken down into smaller particles. Overall, the results indicate that atomization produces smaller and more uniform vesicles, which are beneficial for aerosol delivery. Our study found that the non-atomized vesicles were on average 1.3 µm in size, which differs slightly from the 3.3 µm reported in the literature **[32]**. This discrepancy could be due to the use of phase contrast microscopy, which can more accurately detect smaller vesicle diameters. Despite this difference, our results are consistent with existing knowledge on non-atomized surfactant vesicles, confirming the reliability of our results.

This reduction in size and improvement in homogeneity may potentially increase the clinical efficacy of surfactant therapies, particularly in the treatment of respiratory diseases. Our

analysis is consistent with the existing literature on non-atomized surfactant vesicles and confirms the reliability and relevance of our findings.

1.4. Aerodynamic parameters of atomized surfactant

We monitored the PSD and transmittance of the exogenous surfactant aerosol generated by different Endosurf devices in real time. Initially, high transmittance values indicated low particle generation. After atomization began, the transmittance decreased significantly, indicating aerosol generation. After atomization was completed, the transmission values stabilized and then increased, indicating insufficient particle production. The transmission curve versus time showed a U-shape throughout the process. For each measurement, the "Selected Zone" option was used to focus on the relevant data and exclude the values at the beginning and end of atomization.

Table 4: *Results of* $\boldsymbol{D_{10}}$ $\boldsymbol{D_{50}}$ *and of* $\boldsymbol{D_{90}}$ *after SPRAYTEC analysis.*$D_{10}(\mu m), D_{50}(\mu m), and\ D_{90}(\mu m)$ *were calculated using the SPRAYTEC software. They represent maximal particle size diameter that includes 10%, 50% and 90% of total particles volume, respectively.*

Device	Caption	$D_{10}(\mu m)$	$D_{50}(\mu m)$	$D_{90}(\mu m)$
(4)		20.00	44.21	86.85
(5)		25.50	56.46	120.58
(6)		99.30	180.75	394.27
(7)		97.05	193.96	432.27
(8)		19.31	36.91	66.26
(9)		22.49	43.45	80.05
(10)		74.44	146.53	352.68
(11)		122.29	226.47	441.29
(12)		27.13	52.42	99.65

As shown in **Table 4**, the average D_{10} values for these devices range from 19.31 to 122.29µm, the D_{50} values range from 36.91 to 226.47µm and the D_{90}, values range from 66.26 to 432.27µm. D_{50} and D_{90}, which reflect most of the aerosol particles produced by Endosurf devices, are the most commonly used parameters for evaluating aerosol particle size distribution.

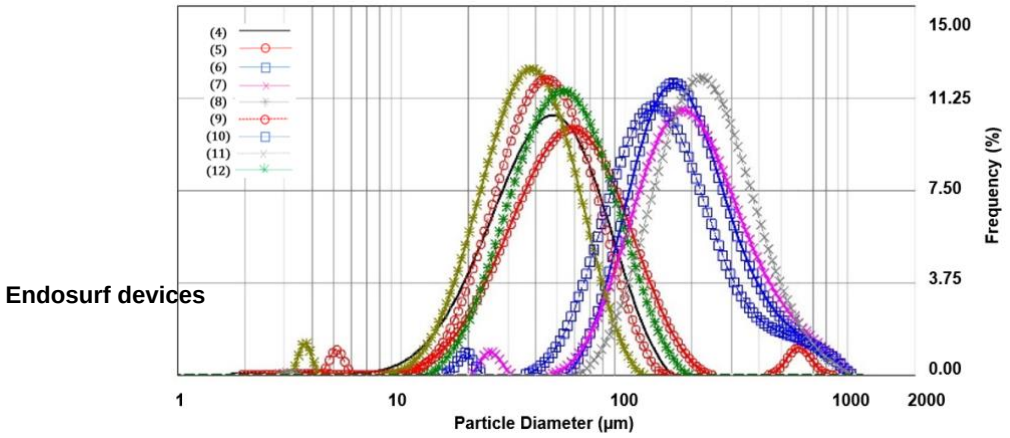

Figure 9*: Particle size distribution of aerosol droplets generated by different devices, measured with the SPRAYTEC.*

The Spraytec system was used to evaluate the performance of nine different Endosurf devices. The key parameters, including D_{10}, D_{50}, D_{90} and transmission, were automatically calculated using the Spraytec software. D_{10}, D_{50} and D_{90} represent the particle size diameters at which 10%, 50% and 90% of the aerosol particles are smaller, respectively. The particle size distribution (PSD) results for each device (labelled 4 to 12).

The figure shows the particle size distribution of the aerosol droplets produced by nine different devices. Each curve in the diagram represents a different device, which is identified by a specific caption.The measurements show that the particle size distribution (PSD) results for each device (labeled 4 to 12) show significant differences, illustrating the differences in aerosol generation between the devices with two different droplet size distributions (**Figure 9**).
Five devices (4, 5, 8, 9 and 12) produce droplets with an average diameter of 46.69 ± 6.9 µm, while the remaining four devices (6, 7, 10 and 11) produce droplets with a smaller average diameter of 186.93 ± 23.29 µm. These differences can be attributed to variations in the manual assembly of the nozzles. It is important to note that manual tightening, even when performed by the same person, can affect the size of the spray orifice. Tightening more can slightly reduce the diameter of the nozzle, resulting in the production of smaller droplets.
We also observe a correlation between the mean droplet diameter and the applied pressure. In particular, a higher pressure leads to smaller droplets (*e.g.*, device 1: 40 bar pressures, mean diameter of 44.21 µm), while a lower pressure leads to larger droplets (*e.g.*, device 8: 20 bar pressure, mean diameter of 226.47 µm).

1.5. *Ex vivo* Imaging of surfactant distribution in the lungs.

Figure 10 shows examples of MRI images taken on isolated thoraxes before and after administration of the surfactant solution. In the images (a) taken before surfactant administration, the lung parenchyma appears hypointense due to its low tissue density compared to the chest musculature.
The images in column (b) taken after surfactant administration show a strong enhancement of signal intensity in the lungs due to the presence of contrast agents in the surfactant solution. The images in column (c) correspond to a maximum intensity projection (MIP) of the 3D MRI image as seen from the front of the thorax. The MIP image (top panel) shows a homogeneous, distal distribution of surfactant in the lung after administration of surfactant with the Endosurf spray device. In comparison, the MIP image taken after instillation of surfactant using the LISA method (lower panel) shows a larger distribution of surfactant in the central airways.

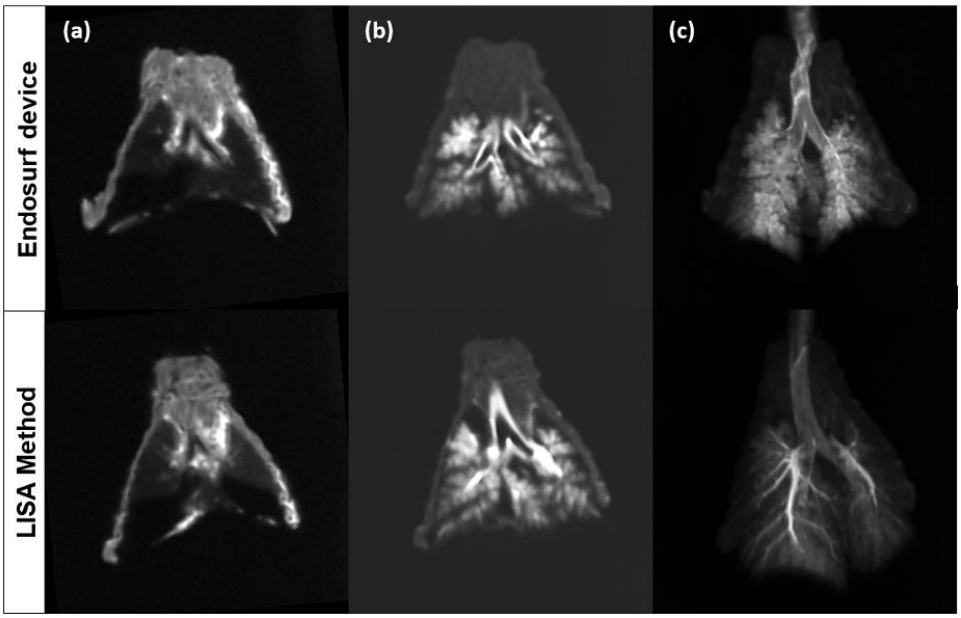

Figure 10. *1 mm thick MR images of the rabbit lung (a) before and (b) after administration of a solution of surfactant and MRI contrast agent using the Endosurf spray device (upper panel) and the LISA method (lower panel). (c)The corresponding maximum intensity projections from the 3D image are shown in column.*

2. CONCLUSION

This study provides important insights into the physico-chemical, rheological and aerodynamic properties of Curosurf® before and after atomization using different Endosurf prototypes. Atomization did not significantly alter the surface tension of the surfactant, confirming its physicochemical stability for therapeutic use. Rheological analysis showed that the viscoelastic properties of the atomized samples were comparable to those of freshly prepared Curosurf®, indicating that atomization preserves the functional integrity of the surfactant. In addition, phase contrast microscopy showed a significant reduction in vesicle size after atomization, accompanied by an increase in the number of smaller vesicles, resulting in a more homogeneous size distribution that allows for better distribution in the lung.

Aerodynamic studies showed that aerosol droplet size varied between the different Endosurf prototypes, with droplet diameter inversely correlated with applied pressure, highlighting the need for optimization of the device to improve aerosol generation efficiency. *Ex vivo* MRI imaging confirmed the uniform distribution of surfactant in lung tissue following delivery *via* the Endosurf spray device, in contrast to the centralized deposition in the airways observed with the LISA method.

In summary, these results confirm the potential of Endosurf devices for effective exogenous surfactant delivery in the treatment of respiratory distress and support further development and clinical optimization.

Data and materials availability

All main data are available in the main text or in the supplementary materials. Complementary information upon data used in the analysis are available on reasonable request to corresponding author.

Supplementary data

S1: *Alveolar instability according to Laplace's law.*

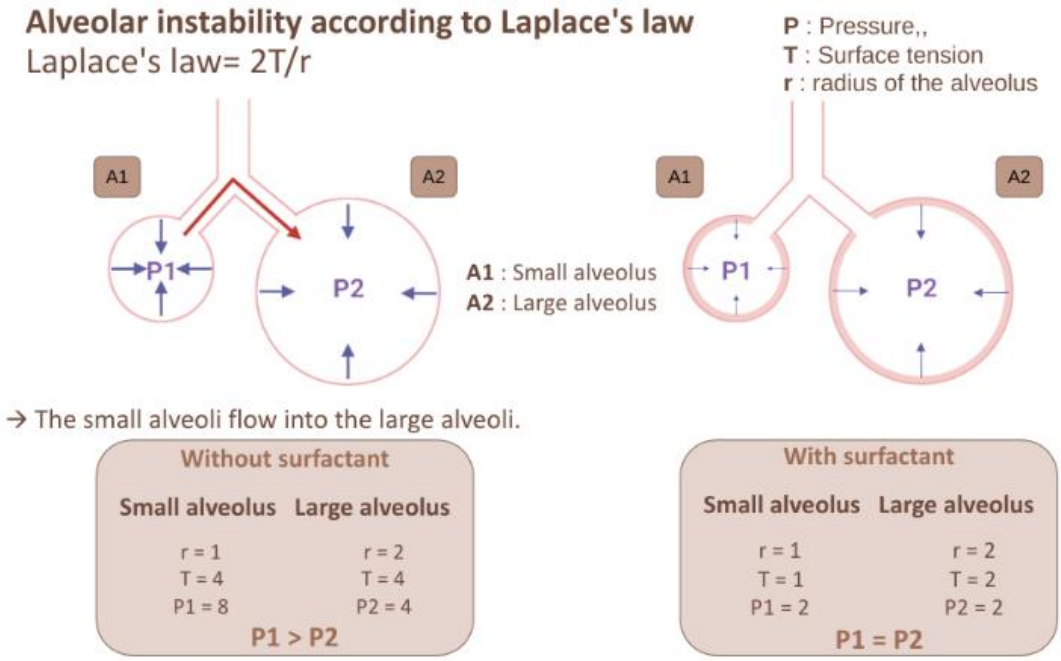

S2: *Droplet Size Distribution - Atomized vs. non-Atomized. The collected data were analyzed in terms of mean, standard deviation, as well as the maximum and minimum droplet diameters, and the distribution of these sizes within each sample. The non-atomized sample was used as a reference to assess the variations observed in the atomized samples.*

Samples	Number of vesicles	Mean (µm)	Standard deviation (µm)	Range (µm)	Size distribution
Non-atomized	250	2.2	2.5	Max :17.0 Min :0.4	118 entre between 0 and 1µm 80 between 1 and 1.5µm 30 between 2 and 3µm 10 between 3 and 4µm 12 between 6 and 18µm
Device (1)	250	1.7	0.9	Max :8.67 Min :0.4	5 between 0 and 0.5µm 40 between 0.5 and 1µm 75 between 1 and 1.5µm 65 between 1.5 and 2µm 35 between 2 and 2.5µm 20 between 2.5 and 3µm 10 between 3 and 9µm
Device (2)	250	1.4	1.4	Max :12.3 Min :0.4	60 between 0 and 0.5µm 70 between 0.5 and 1µm 40 between 1 and 1.5µm 30 between 1.5 and 2µm 20 between 2 and 2.5µm 30 between 2.5 and 15µm
Device (3)	250	0.7	0.5	Max :4.7	5 between 0 and 0.2µm

				Min :0.2	70 between 0.2 and 0.4µm 90 between 0.4 and 0.6µm 50 between 0.6 and 0.8µm 30 between 1 and 1.2µm 5 between 1.2 and 4.8µm

REFERENCES

[1] Krajewski P, Pomianek T, Truszkowski K, Wieckowska K, Gorska M, Wielgos M. Respiratory distress syndrome in preterm infants: possible impact of surfactant application techniques. Ginekol Pol. 2022 ;93(9) :750-755

[2] Krajewski P, Pomianek T, Truszkowski K, Wieckowska K, Gorska M, Wielgos M. Respiratory distress syndrome in preterm infants: possible impact of surfactant application techniques. Ginekol Pol. 2022 ;93(9) :750-755.

[3] Avery ME, Mead J: Surface properties in relation to atelectasis and hyaline membrane disease. Am J Dis Child 1959 ;97 :517-523.

[4] Curstedt, T., Halliday, H. L., & Speer, C. P. (2015). A Unique Story in Neonatal Research: The Development of a Porcine Surfactant. Neonatology, 107(4), 321–329. doi :10.1159/000381117

[5] Weaver TE, Nogee LM, Jobe AH. Tensioactif pendant le développement pulmonaire. Dans : Jobe AH, Whitsett JA, Abman SH, éd. *Développement pulmonaire fœtal et néonatal : corrélations cliniques et technologies pour l'avenir* . Cambridge University Press ; 2016 : 141-163.

[6] Le manuel MSD, Nouveau née prématurés Par Arcangela Lattari Balest , MD, University of Pittsburgh, School of Medicine Revue/Révision complète oct. 2022, Consulté le 1 février 2023

[7] Fanny Mousseau, thèse de doctorat de physique. Le surfactant pulmonaire, une barrière déterminante de la réponse des cellules à l'exposition aux nanoparticules. 26 Janvier 2017

[8] Bajaj P, Harris JF, Huang JH, Nath P, Iyer R. Advances and Challenges in Recapitulating Human Pulmonary Systems: At the Cusp of Biology and Materials. ACS Biomater Sci Eng. 2016 Apr 11;2(4):473-488. doi: 10.1021/acsbiomaterials.5b00480. Epub 2016 Mar 14. PMID: 33465851.

[9] Gillich A, Zhang F, Farmer CG, Travaglini KJ, Tan SY, Gu M, Zhou B, Feinstein JA, Krasnow MA, Metzger RJ. Capillary cell-type specialization in the alveolus. Nature. 2020 Oct;586(7831):785-789. doi: 10.1038/s41586-020-2822-7. Epub 2020 Oct 14. PMID: 33057196; PMCID: PMC7721049.

[10] Pinheiro JM, Santana-Rivas Q, Pezzano C. Randomized trial of laryngeal mask airway versus endotracheal intubation for surfactant delivery. J Perinatol 2016;36:196–201

[11] Ochs M, Nyengaard JR, Jung A, Knudsen L, Voigt M, Wahlers T, Richter J, Gundersen HJ. The number of alveoli in the human lung. Am J Respir Crit Care Med. 2004 Jan 1;169(1):120-4. doi: 10.1164/rccm.200308-1107OC. Epub 2003 Sep 25. PMID: 14512270.

[12] Donda, K., Vijayakanthi, N., Dapaah-Siakwan, F., Bhatt, P., Rastogi, D., & Rastogi, S. (2019). Trends in epidemiology and outcomes of respiratory distress syndrome in the United States. Pediatric Pulmonology, 54(4), 405–414. doi :10.1002/ppul.24241

[13] Waisman, D.; Danino, D.; Weintraub, Z.; Schmidt, J.; Talmon, Y. Nanostructure of the Aqueous Form of Lung Surfactant of Different Species Visualized by Cryo-Transmission Electron Microscopy. Clinical Physiology and Functional Imaging 2007, 27, 375-380. DOI: 10.1111/j.1475-097X.2007.00763.x.

[14] Ciutara, C. O.; Zasadzinski, J. A. Bilayer aggregate microstructure determines viscoelasticity of lung surfactant suspensions. Soft Matter 2021, 17, 5170-5182, 10.1039/D1SM00337B. DOI: 10.1039/D1SM00337B.

[15] Mousseau, F.; Oikonomou, E. K.; Vacher, A.; Airiau, M.; Mornet, S.; Berret, J.-F. Revealing the Pulmonary Surfactant Corona on Silica Nanoparticles by Cryo-Transmission Electron Microscopy. Nanoscale Advances 2020, 2, 642-647. DOI: 10.1039/c9na00779b.

[16] Mousseau, F.; Berret, J. F. The Role of Surface Charge in the Interaction of Nanoparticles with Model Pulmonary Surfactants. Soft Matter 2018, 14, 5764-5774. DOI: 10.1039/c8sm00925b.

[17] King, D. M.; Wang, Z. D.; Kendig, J. W.; Palmer, H. J.; Holm, B. A.; Notter, R. H. Concentration-Dependent, Temperature-Dependent Non-Newtonian Viscosity of Lung Surfactant Dispersions. Chemistry and Physics of Lipids 2001, 112, 11-19. DOI: 10.1016/s0009-3084(01)00150-5.

[18] King, D. M.; Wang, Z. D.; Palmer, H. J.; Holm, B. A.; Notter, R. H. Bulk Shear Viscosities of Endogenous and Exogenous Lung Surfactants. American Journal of Physiology: Lung Cellular and Molecular Physiology 2002, 282, L277-L284. DOI: 10.1152/ajplung.00199.2001.

[19] Lu, K. W.; Perez-Gil, J.; Taeusch, H. W. Kinematic Viscosity of Therapeutic Pulmonary Surfactants with Added Polymers. Biochimica et Biophysica Acta Biomembranes 2009, 1788, 632-637. DOI: 10.1016/j.bbamem.2009.01.005.

[20] Ciutara, C. O.; Zasadzinski, J. A. Bilayer aggregate microstructure determines viscoelasticity of lung surfactant suspensions. Soft Matter 2021, 17, 5170-5182, 10.1039/D1SM00337B. DOI: 10.1039/D1SM00337B.

[21] Thai, L.-P.-A.; Mousseau, F.; Oikonomou, E.; Radiom, M.; Berret, J.-F. On the Rheology of Pulmonary Surfactant: Effects of Concentration and Consequences for the Surfactant Replacement Therapy. Colloids and Surfaces B: Biointerfaces 2019, 178, 337-345. DOI: 10.1016/j.colsurfb.2019.03.020.

[22] Thai, L.-P.-A.; Mousseau, F.; Oikonomou, E.; Radiom, M.; Berret, J.-F. Effect of Nanoparticles on the Bulk Shear Viscosity of a Lung Surfactant Fluid. ACS Nano 2020, 14, 466-475. DOI: 10.1021/acsnano.9b06293.

[23] Berret, J. F. Comment on "Bilayer aggregate microstructure determines viscoelasticity of lung surfactant suspensions" by C. O. Ciutara and J. A. Zasadzinski, Soft Matter, 2021, 17, 5170-5182. Soft Matter 2022, 18, 8514-8519 DOI: 10.1039/d2sm00653g.

[24] Perez-Gil J, Weaver TE. Pulmonary surfactant pathophysiology: current models and open questions. Physiology (Bethesda). 2010 Jun;25(3):132-41. doi: 10.1152/physiol.00006.2010. PMID: 20551227.

[25] McCarthy SD, González HE, Higgins BD. Future Trends in Nebulized Therapies for Pulmonary Disease. J Pers Med. 2020 May 10;10(2):37. doi: 10.3390/jpm10020037. PMID: 32397615; PMCID: PMC7354528.

[26] Sardesai S, Biniwale M, Wertheimer F, Garingo A, Ramanathan R. Evolution of surfactant therapy for respiratory distress syndrome: past, present, and future. Pediatr Res. 2017;81(1-2):240-248. doi:10.1038/pr.2016.203

[27] Verder H, Agertoft L, Albertsen P, et al. [Surfactant treatment of newborn infants with respiratory distress syndrome primarily treated with nasal continuous positive air pressure. A pilot study]. Ugeskr Laeger 1992;154:2136–9.

[28] Leone F, Trevisanuto D, Cavallin F, Parotto M, Zanardo V. Efficacy of INSURE during nasal CPAP in preterm infants with respiratory distress syndrome. Minerva Pediatr 2013;65:187–92.

[29] Kanmaz HG, Erdeve O, Canpolat FE, Mutlu B, Dilmen U. Surfactant administration via thin catheter during spontaneous breathing: randomized controlled trial. Pediatrics 2013;131:e5029

[30]Patent#FR3105004https://worldwide.espacenet.com/publicationDetails/biblio?FT=D&date=20210625&DB=&locale=fr_EP&CC=FR&NR=3105004A1&KC=A1&ND=4

[31] F. Mousseau, J.-F. Berret, E.K. Oikonomou, Design and Applications of a Fluorescent Labeling Technique for Lipid and Surfactant Preformed Vesicles, *ACS Omega* **4**, 10485-10493 (2019).

[32] L.-P.-A. Thai, F. Mousseau, E. Oikonomou, M. Radiom, J.-F. Berret, On the Rheology of Pulmonary Surfactant: Effects of Concentration and Consequences for the Surfactant Replacement Therapy, *Colloids and Surfaces B: Biointerfaces* **178**, 337-345 (2019).

[33] Schindelin J, Arganda-Carreras I, Frise E, Kaynig V, Longair M, Pietzsch T, Preibisch S, Rueden C, Saalfeld S, Schmid B, Tinevez JY, White DJ, Hartenstein V, Eliceiri K, Tomancak P, Cardona A. Fiji: an open-source platform for biological-image analysis. Nat Methods. 2012 Jun 28;9(7):676-82. doi: 10.1038/nmeth.2019. PMID: 22743772; PMCID: PMC3855844.

[34] Montigaud Y, Périnel S, Dubus JC, Leclerc L, Suau M, Goy C, Clotagatide A, Prévôt N, Pourchez J. Development of an ex vivo respiratory pediatric model of bronchopulmonary dysplasia for aerosol deposition studies. Sci Rep. 2019 Apr 5;9(1):5720. doi: 10.1038/s41598-019-42103-2. PMID: 30952897; PMCID: PMC6450907

[35] Crémillieux Y, Montigaud Y, Bal C, Pinaud N, Pham V, Perinel S, Natuzzi M, Lux F, Tillement O, Ichinose N, Zhang B, Pourchez J. Three-dimensional quantitative MRI of aerosolized gadolinium-based nanoparticles and contrast agents in isolated ventilated porcine lungs. Magn Reson Med. 2020 May;83(5):1774-1782. doi: 10.1002/mrm.28041. Epub 2019 Oct 25. PMID: 31654446.
[36] Dani C, Martelli E, Tronchin M, et al. Bilirubin influence on oxidative lung damage and surfactant surface tension properties. *Pediatr Pulmonol*. 2004;38(3):179-185. doi:10.1002/ppul.20045
[37] H.H. Winter, F. Chambon, Analysis of Linear Viscoelasticity of a Cross-Linking Polymer at the Gel Point, *Journal of Rheology* **30**, 367-382 (1986).
[38] M. In, R.K. Prud'homme, Fourier transform mechanical spectroscopy of the sol-gel transition in zirconium alkoxide ceramic gels, *Rheologica Acta* **32**, 556-565 (1993).
[39] P. Coussot, Rheophysics of pastes: a review of microscopic modelling approaches, *Soft Matter* **3**, 528-540 (2007).
[40] C.O. Ciutara, J.A. Zasadzinski, Bilayer aggregate microstructure determines viscoelasticity of lung surfactant suspensions, *Soft Matter* **17**, 5170-5182 (2021).
[41] J.F. Berret, Comment on "Bilayer aggregate microstructure determines viscoelasticity of lung surfactant suspensions" by C. O. Ciutara and J. A. Zasadzinski, Soft Matter, 2021, 17, 5170-5182, *Soft Matter* **18**, 8514-8519 (2022).
[42] R.G. Larson, *The Structure and Rheology of Complex Fluids*, Oxford University Press, New York, 1998.
[43] D.M. King, Z.D. Wang, H.J. Palmer, B.A. Holm, R.H. Notter, Bulk Shear Viscosities of Endogenous and Exogenous Lung Surfactants, *American Journal of Physiology: Lung Cellular and Molecular Physiology* **282**, L277-L284 (2002).
[44] L.-P.-A. Thai, F. Mousseau, E. Oikonomou, M. Radiom, J.-F. Berret, Effect of Nanoparticles on the Bulk Shear Viscosity of a Lung Surfactant Fluid, *ACS Nano* **14**, 466-475 (2020).
[45] K.W. Lu, J. Perez-Gil, H.W. Taeusch, Kinematic Viscosity of Therapeutic Pulmonary Surfactants with Added Polymers, *Biochimica et Biophysica Acta Biomembranes* **1788**, 632-637 (2009).
[46] D.M. King, Z.D. Wang, J.W. Kendig, H.J. Palmer, B.A. Holm, R.H. Notter, Concentration-Dependent, Temperature-Dependent Non-Newtonian Viscosity of Lung Surfactant Dispersions, *Chemistry and Physics of Lipids* **112**, 11-19 (2001).